Eur. J. Mineral.
2015, **27**, 793–803
Published online 26 August 2015

Perettiite-(Y), $Y^{3+}{}_2Mn^{2+}{}_4Fe^{2+}[Si_2B_8O_{24}]$, a new mineral from Momeik, Myanmar

ROSA MICAELA DANISI[1,*], THOMAS ARMBRUSTER[1], EUGEN LIBOWITZKY[2], HAO A.O. WANG[3], DETLEF GÜNTHER[3], MARIKO NAGASHIMA[4], ERIC REUSSER[5] and WILLY BIERI[6]

[1] Mineralogical Crystallography, Institute of Geological Sciences, University of Bern, Freiestrasse 3, 3012 Bern, Switzerland
*Corresponding author, e-mail: rosa.danisi@krist.unibe.ch
[2] Institut für Mineralogie und Kristallographie, Universität Wien-Geozentrum, Althanstrasse 14, 1090 Wien, Austria
[3] ETH Zurich, Laboratory of Inorganic Chemistry, Vladimir-Prelog-Weg 1, 8093 Zürich, Switzerland
[4] Graduate School of Science and Engineering, Yamaguchi University, Yamaguchi 753–8512, Japan
[5] Institut für Geochemie und Petrologie, ETHZ, Clausiusstrasse 25, 8082 Zürich, Switzerland
[6] GRS Gemresearch Swisslab AG, Baldismoostrasse 14, 6043 Adligenswil, Switzerland

Abstract: The new mineral perettiite-(Y), end-member formula $Y^{3+}{}_2Mn^{2+}{}_4Fe^{2+}[Si_2B_8O_{24}]$, from pegmatites in the region of Momeik, north of Mogok, Myanmar, occurs as yellow needles enclosed in phenakite crystals. The mineral was named after the mineralogist and gemologist Dr. Adolf Peretti. The empirical formula using LA-ICP-MS data (based on 24 O *pfu*) is $Y_{2.06}Ln_{0.53}Zr_{0.02}Th_{0.01}Mn_{3.24}Ca_{0.38}Fe_{0.71}Mg_{0.07}Al_{0.11}Li_{0.22}Si_{1.95}B_{7.44}Be_{0.31}O_{24}$. Calculation of the H_2O content using IR absorption data yields a maximum hydroxyl/water content equivalent to 0.1 wt.% H_2O. The strongest lines in the powder pattern [*d* in Å (*I*$_{meas.}$) (*hkl*)] are 4.63 (52) (010), 4.08 (28) (301, 103), 3.74 (20) (210), 3.05 (100) (113, 311, 303), 2.64 (67) (410, 014), 2.54 (60) (313), 2.12 (23) (600, 006), 1.87 (33) (420, 024), 1.84 (52) (415, 323), 1.57 (20) (026, 620), 1.44 (25) (133, 331). The perettiite-(Y) crystals show a tetragonal X-ray diffraction pattern but the structure could only be solved as a 50/50 pseudo-merohedral orthorhombic twin with the *a* and *c* axes having the same length. The structure, refined to $R1 = 0.017$ (space group *Pmna* with $a = 12.8252(5)$, $b = 4.6187(2)$, $c = 12.8252(5)$ Å, $V = 759.71(5)$ Å^3, $Z = 2$), is characterized by two eight-coordinated sites: one dominated by Y and lanthanoids (Ln) and the other by Mn^{2+} (with additional Ca^{2+} and Y^{3+}). An octahedral site is occupied by (Fe^{2+}, Mg) with additional Li^+. These cation sites form an interlayer between two tetrahedral sheets of $Si_2B_8O_{24}$ composition. Boron shows minor replacement by beryllium. Arrangement of 4-, 5- and 8-membered rings within (010) form the borosilicate tetrahedral sheets.

Perettiite-(Y) is brittle, with irregular fracture and (010) cleavage; the estimated Mohs hardness is ~ 7. Using the empirical formula, the density was estimated to be 4.533 g cm^{-3}. Perettiite-(Y) is biaxial, $\alpha = 1.82(1)$, $\gamma = 1.84(1)$ (589 nm).

Key-words: Perettiite-(Y); $Y^{3+}{}_2Mn^{2+}{}_4Fe^{2+}[Si_2B_8O_{24}]$; crystal structure; new mineral; borosilicate; Momeik; Myanmar.

Introduction

The region of Momeik, north-central Myanmar, is located in the well-known gem-producing area of the Mogok metamorphic belt (MMB). The MMB extends over 1500 km stretching N-S through Myanmar. It is approximately 50 km wide and consists of high-grade metamorphic marbles, schists and gneisses that are intruded by granitoids and pegmatites (Searle *et al*., 2007). Ruby- and spinel-bearing marbles interlayered with gneisses near Mogok are famous for providing the world's finest rubies (Keller, 1983; Peretti, 2013).

Perettiite-(Y) was first recognized by Peretti as inclusions in one of about a dozen cm-size idiomorphic phenakite crystals, which he purchased in the Mogok gem market in 2007. This discovery initiated a field trip to Mogok in 2014 at which a stock of approximately 10000 corresponding phenakite crystals, indicated as coming from the Molo area (north of Momeik), was acquired by Peretti from a local gemologist and dealer in Mogok. Optical microscope investigations revealed about 15 phenakite crystals containing yellow needle-like inclusions, afterwards identified as perettiite-(Y). During the visit in 2014, it was impossible to gain access to the mines of the Molo area due to the ongoing civil war in Myanmar. Nevertheless, a field geologist that worked in this region confirmed the provenance of the phenakite samples that are found in isolated pockets of granitic pegmatites intruding large peridotite bodies. In the same area,

DOI: 10.1127/ejm/2015/0027-2483 0935-1221/15/0027-2483 $ 4.95

''mushroom tourmaline'' (Falster *et al.*, 2007; Lussier *et al.*, 2008) and bismutotantalite–stibiotantalite–stibiocolumbite aggregates (Novak *et al.*, 2008) were reported.

Two phenakite crystals containing yellow needle-like inclusions were subsequently sent to us for identification. Preliminary EDX (Energy dispersive X-ray) analysis of the inclusions showed the Y-rich chemical composition that aroused our interest and encouraged us to collect single-crystal X-ray diffraction data. The results allowed us to describe a new mineral species named in honor of Dr. Adolf Peretti (born in 1957), mineralogist and head of GRS Gemresearch Swisslab AG. Dr. Peretti is highly engaged in the study of minerals and gemstones, and he first recognized ''perettiite-(Y)'' as inclusions in the phenakite. The mineral and its name have been approved by the IMA Commission on New Minerals, Nomenclature and Classification (IMA 2014–109). Holotype material is deposited in the collection of the Museum of Natural History Bern, Switzerland, specimen number NMBE-43035.

Occurrence and paragenesis

Granitic pegmatites in the vicinity of Khetchel, Molo area, north of Momeik (Myanmar) are the source of perettiite-bearing phenakite crystals (Fig. 1). The type locality coordinates are 23°18'35'' N/96°52' E. These pegmatites intrude a large peridotite body of approximately 5–10 km^2. Perettiite-bearing phenakite forms dominantly prismatic and mostly twinned crystals up to a few cm in length. It occurs in a typical pegmatitic assemblage together with crystals of quartz, feldspars and schorl. Mushroom and botryoidal tourmalines, hambergite and petalite are reported 300 m northwest from the perettiite-(Y) type locality. Beryl has been found in the varieties aquamarine and morganite. Pollucite and danburite crystals up to several centimeters in size occur in miarolitic cavities. Topaz, almandine–spessartine, biotite, magnetite, lepidolite, hübnerite–ferberite, and cassiterite have been described (Falster *et al.*, 2007). Overall, the paragenesis bears considerable similarity to high-B and high-Cs pegmatites (Zaw, 1998).

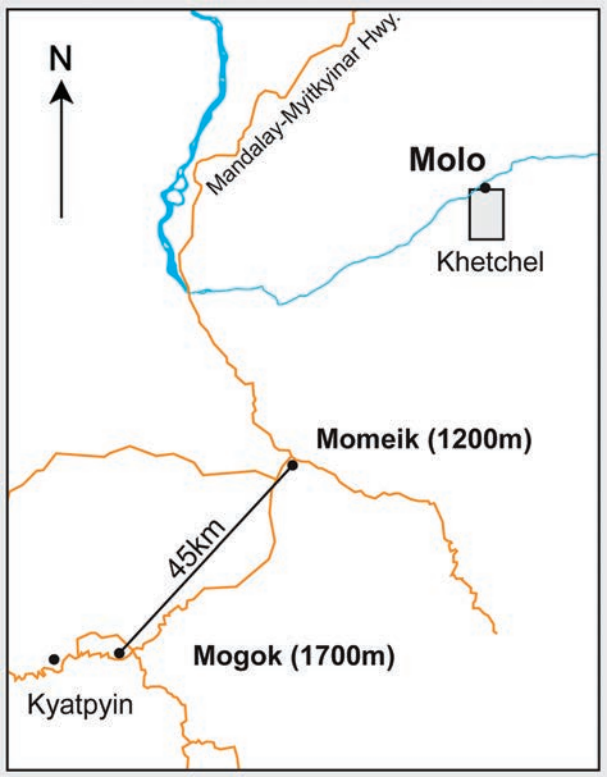

Fig. 1. Localization of the Molo area (gray box), type locality of perettiite-(Y) (modified from Peretti *et al.*, 2015).

Perettiite-(Y) occurs as yellow needles enclosed in transparent colorless phenakite crystals. Other inclusions in phenakite, analyzed by us using single-crystal X-ray diffraction, are: schorl, tusionite, columbite-(Mn), albite, fluorapatite, lazulite. The shape of perettiite-(Y) needles with an obviously broken base and tapered tip suggests that the needles predate phenakite and were randomly overgrown by phenakite during pegmatite evolution.

Physical and optical properties

Yellow, transparent, tapered needles of perettiite-(Y) enclosed in phenakite are few mm in length and up to 0.2 mm in diameter (Fig. 2). Crystal (010) cross-sections mimic tetragonal symmetry but are intimately twinned, showing under crossed polarizers a characteristic hour-glass pattern (similar to apophyllite) with undulatory extinction (Fig. 2). Perettiite-(Y) is brittle, with irregular fracture; the estimated Mohs hardness determined (sample 1) by microindentation test is 7 (VHN load 300 g, range 100–110, mean 100 kg mm^{-2}). It occurs as crystals acicular along [010], the forms {100} and {001} are observed. Cleavage is good parallel to (010). The streak is colorless, the luster is vitreous. Density could not be measured due to intergrowth with phenakite and crystal zoning. Using the empirical formula, measured unit-cell volume and *Z*, calculated density is to be 4.533 g cm^{-3}. Several other estimates of density were attempted. Perhaps the most reliable is that from structure refinement including determination of site occupancies (4.35 g cm^{-3}). The LA-ICP-MS (Laser ablation - inductively coupled plasma - mass spectrometry) analytical data combined with cell parameters normalized to Si + B = 10 atoms per formula unit (*apfu*) give 4.67 g cm^{-3}. The same data normalized to 24 O give 4.47 g cm^{-3} whereas LA-ICP-MS analytical data with Y_2O_3 values taken from electron microprobe data normalized to 17 cations yield 4.45 g cm^{-3}. Perettiite-(Y) is biaxial, $\alpha = 1.82(1)$, $\gamma = 1.84(1)$ (589 nm). Due to intimate twinning, the crystal appears conoscopically uniaxial with diffuse isogyre cross, thus the optical character 2*V* and β could not be estimated. The determined α and γ values represent minimum and maximum refractive indices. From these two values the average refractive index may be estimated to be 1.83.

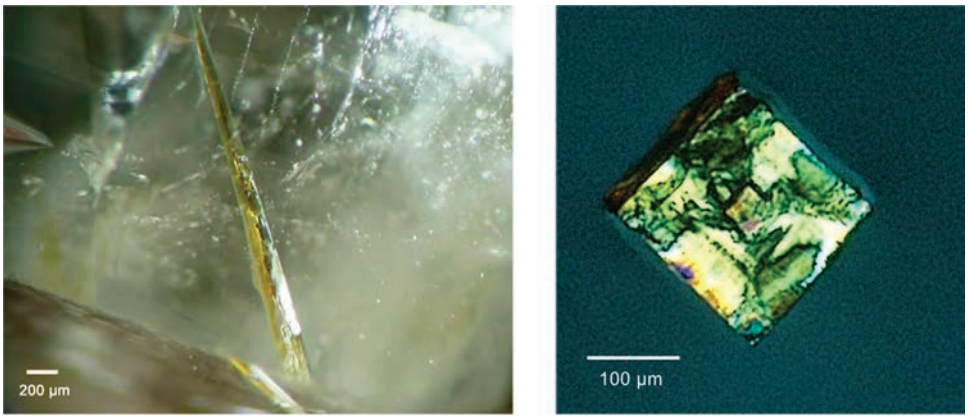

Fig. 2. **(a):** Perettiite-(Y) inclusion (light yellow needle *ca.* 2 mm long and 0.2 mm thick) in phenakite. **(b):** A fragment of the needle (*ca.* 0.2 mm in all dimensions) was liberated by crushing the phenakite host crystal. The picture was taken under crossed polarizers in oil and the crystal is oriented with the needle axis parallel to the light beam.

Dispersion was not estimated due to twinning. No pleochroism was observed.

Chemical composition

Electron-microprobe analyses (EMPA) were performed in wavelength dispersive mode using two different setups on two samples, leading to 25 point analyses (10 + 15 measurements). Sample 1 was analyzed with a JEOL JXA 8200 electron microprobe (Institut für Geochemie und Petrologie, ETHZ). The analytical conditions were: excitation voltage 15kV, specimen current 20 nA, beam diameter ~1 µm. The counting times on peak were between 40 and 80 s. The same total time was used for background measurement. Standards used were synthetic oxides (YAG, Mn-oxide, REE-aluminates) and pure natural silicates. Sample 2 was analyzed with a JEOL JXA-8230 machine (Yamaguchi University, Japan). The analytical conditions were: excitation voltage 15 kV, specimen current 20 nA, beam diameter 10 µm, 10 s counting time. X-ray lines, analyzer crystals, and standard materials are listed in Table S1 (freely available as Supplementary Material linked to this article on the GSW website of the journal: http://eurjmin.geoscienceworld.org/). The ZAF (atomic number - absorption - fluorescence) correction-method (Pouchou & Pichoir, 1984) was used for all elements. Results are given in Table 1. The EMPA data for MgO, Al_2O_3, CaO, FeO and MnO are in good agreement with LA-ICP-MS results.

The LA-ICP-MS analyses were carried out on sample 1 using a 193 nm ArF Excimer system (GeoLasQ, Lambda Physik, Göttingen, Germany) together with ELAN 6100 DRC quadrupole ICP-MS (Perkin Elmer SCIEX, Canada). The laser fluence was kept between 24 and 26 J/cm^2 at 10 Hz repetition rate. A 10 µm laser spot was focused on the sample surface, and during ablation the laser spot was kept at the same position on the sample (hole drilling mode). The LA-ICP-MS setup was routinely tuned for optimized performance. A dwell time of 10 ms was applied to every isotope of interest. More than 60 s transient signals (30 s background + >30 s LA signal) were acquired for all measurements. In total, more than 64 isotopes were measured and externally calibrated using NIST610 standard reference material. Data evaluation was done using the in-house-built software StalQuant 4.1 based on the standard procedure (Longerich *et al*., 1996). Assuming all measured analytes in their oxides form in perettiite-(Y), we normalized the total concentration of all oxides to 100 %, which resulted in an internal-standard-independent quantification (Guillong *et al*., 2005).

However, Y_2O_3 contents determined by LA-ICP-MS were *ca.* 3 wt.% higher than EMPA results, which could be a result

Table 1. Chemical data for perettiite-(Y).

Constituent	LA-ICP-MS wt.%	Range	EMP averages for 2 samples, wt.%*
Li_2O	0.32	0.24–0.38	
BeO	0.75	0.66–0.82	
B_2O_3	24.86	24.61–25.12	
MgO	0.27	0.23–0.29	0.56, 0.44
Al_2O_3	0.56	0.48–0.62	
SiO_2	11.26	10.42–12.02	11.88, 11.94
CaO	2.02	1.82–2.27	1.66, 2.00
MnO	22.06	21.04–23.56	22.95, 21.20
FeO	4.89	4.62–5.15	4.62, 4.52
Y_2O_3	22.32	21.81–23.04	19.00, 20.99
ZrO_2	0.19	0.17–0.20	
Sm_2O_3	0.24	0.23–0.27	
Gd_2O_3	0.71	0.66–0.80	n.d., 1.42
Tb_2O_3	0.29	0.28–0.31	
Dy_2O_3	2.62	2.45–2.75	n.d, 2.14
Ho_2O_3	0.53	0.50–0.55	
Er_2O_3	1.78	1.73–1.92	n.d., 1.71
Tm_2O_3	0.33	0.32–0.37	
Yb_2O_3	2.85	2.59–3.24	n.d., 2.68
Lu_2O_3	0.38	0.35–0.42	
ThO_2	0.33	0.30–0.41	
Total	99.56		

*Note: samples 1 and 2; n.d.: not determined.

Table 2. Comparison of perettiite-(Y) stoichiometry (*apfu*) resulting from different analytical techniques.

	LA-ICP-MS	LA-ICP-MS*	XRD**
Y	2.06	1.78	1.94
Ln	0.53	0.54	0.36
Σ (Y+Ln)	2.59	2.32	2.30
Zr	0.02	0.02	
Th	0.01	0.02	
Mn	3.24	3.29	3.34
Ca	0.38	0.38	0.36
Σ (Zr+Th+Mn+Ca)	3.65	3.71	3.7
Σ 8-coordinated sites	6.24	6.03	6
Li	0.22	0.23	0.2
Fe	0.71	0.72	0.49
Mg	0.07	0.07	0.31
Al	0.11	0.12	
Σ 6-coordinated sites	0.93	0.95	1
Si	1.95	1.98	2
B	7.44	7.56	7.6
Be	0.31	0.32	0.4
Σ 4-coordinated sites	9.7	9.86	10
O	24	23.89	24

*normalized to the Y_2O_3 content obtained from electron-microprobe analyses.
**refined site occupancies from single-crystal X-ray structure refinement.

of the matrix-effect because of an applied non-matrix-matched NIST610 standard (~70 wt.% SiO_2, 500 mg/kg nominal trace-element concentrations for Y and lanthanoids) (Kroslakova & Günther, 2007). Calculations based on the results of the structure refinement (see below) indicate that the lower Y_2O_3 values are in better agreement with the stoichiometry of the structure having 17 cations and 24 O *apfu* (Table 2). In addition, the lanthanoid concentrations were considerably lower when refined by single-crystal X-ray methods (Table 1) as a consequence of the above mentioned matrix-effect. The lanthanoid distribution is Yb > Dy > Er > Gd > Ho > Lu > Tm > Tb > Sm. The simplified formula is $(Y,Yb)_2(Mn,Ca)_4(Fe,Mg,Li)(Si_2B_8O_{24})$ and the end-member formula is $Y^{3+}{}_2Mn^{2+}{}_4Fe^{2+}[Si_2B_8O_{24}]$.

Raman and FTIR spectroscopy

The single crystal of perettiite-(Y) used for spectroscopic investigations was an approximately cube-shaped fragment with a size of ~ 0.2 × 0.2 × 0.2 mm that was obtained as a cross section from a several mm long spindle-shaped individual (sample 2). The crystal showed a yellow brownish color and, except for the turbid central part (along the spindle axis), was optically clear in most regions.

Micro-Raman spectroscopy

Raman spectra were collected by using a Renishaw RM1000 confocal edge filter-based micro-Raman system. The 488 nm excitation line of a ~ 20 mW Ar-ion laser was focused with a 50 ×/0.75 objective lens on the sample surface. The back-scattered radiation (180° configuration) was analyzed with a 1200 lines/mm grating monochromator. Raman intensities were acquired for 2 × 60 s (spectral range ~ 20–4000 cm^{-1}, continuous grating scan mode) and 30 × 120 s (~ 50–1660 cm^{-1}, static grating mode) with a thermo-electrically cooled CCD array detector. The spectral resolution of the system (''apparatus function'') was 5–6 cm^{-1}, the wavenumber accuracy was ±1 cm^{-1} (both calibrated with the Rayleigh line and the 520.5 cm^{-1} line of a Si standard). The confocal setup limited the spatial (lateral and depth) resolution to 2–3 μm. Instrument control and data acquisition were done with Grams/32 software (Galactic Ind. Corp.).

Raman spectra exhibit multiple and quite intense luminescence emission lines (1200–1600 and 1800–2700 cm^{-1}) probably caused by the content of lanthanoids (Fig. 3). However, below 1200 cm^{-1} comparably weak Raman bands are visible. Only a long-term exposure (see above) yields an appropriate signal to noise ratio (Fig. 3 inset) to identify vibrations at *ca.* 1000, 700–800 and < 500 cm^{-1} that can be well compared to common borosilicate stretching, bending and lattice modes (*e.g.* datolite, Farmer, 1974). The Raman spectra do not indicate any stoichiometric water/hydroxyl content (missing bands in the 3000–3700 cm^{-1} region), but minor amounts cannot be excluded due to the low sensitivity of Raman spectroscopy to hydrous species. The band at *ca.* 3850 cm^{-1} is probably another luminescence line. Spectra from the core *vs.* rim of the sample did not show any differences.

FTIR micro-spectroscopy

Single-crystal micro-FTIR spectra were acquired from 550 to 7500 cm^{-1} on a Bruker Tensor 27 FTIR spectrometer connected to a Bruker Hyperion IR microscope.

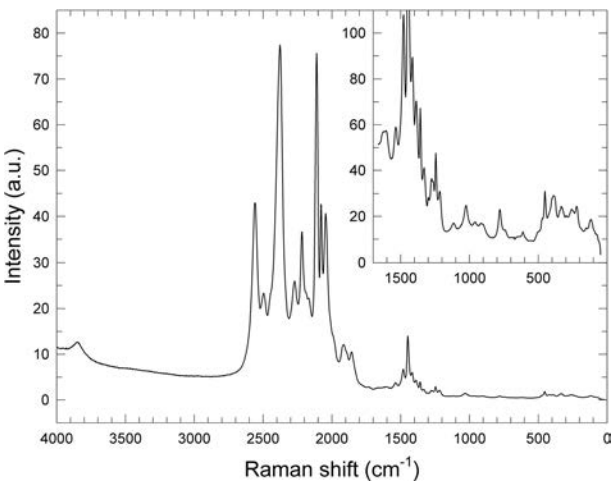

Fig. 3. Micro-Raman spectra (488 nm excitation) of a perettiite-(Y) single-crystal. The full spectrum is dominated by multiple and strong luminescence lines. Only a long term exposure (inset) reveals the Raman bands at <1200 cm^{-1} with acceptable signal-to-noise ratio.

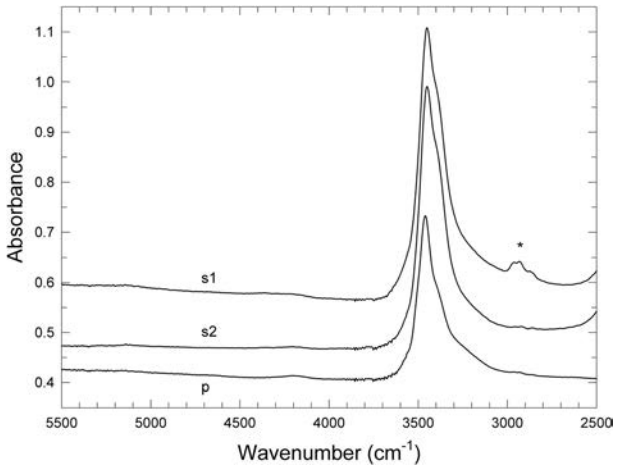

Fig. 4. FTIR micro-spectra of a perettiite-(Y) single-crystal reveal an intense O–H stretching band at 2750–3750 cm^{-1}. IR beam directions s and p indicate ''senkrecht'' (perpendicular) and parallel to the crystal spindle-axis, respectively. Spectra are vertically offset for better visibility. The asterisk marks C–H stretching vibrations from an organic impurity.

The system was equipped with a glo(w)bar MIR light source, a KBr beam splitter, a 15 ×/0.4 Cassegrain type condenser and objective, and a liquid-nitrogen-cooled MCT detector. To avoid any influence from stray light, the perettiite-(Y) single-crystal was placed on a 100 μm circular metal aperture. Sample and background (empty aperture) spectra were averaged from 128 scans at 4 cm^{-1} spectral resolution. Instrument control and data handling were performed with OPUS 5.5 software (Bruker Optik GmbH).

The spectra obtained (Fig. 4) exhibit an intense band in the region of the fundamental O–H stretching vibrations (OH^- or H_2O) at *ca.* 2750–3750 cm^{-1}. At higher wavenumbers, a very weak hump at *ca.* 4200 cm^{-1} is characteristic of a combination band of hydroxyl groups (Rossman, 1988), an even smaller one at *ca.* 5200 cm^{-1} may indicate the combination mode of H_2O molecules (fluid inclusions in the turbid areas?). Below 2500 cm^{-1} the absorption increases tremendously, caused by the first overtone and the fundamental modes of the borosilicate matrix.

A quantitative calculation of the H_2O content using the general calibration of Libowitzky & Rossman (1997) yields a maximum hydroxyl/water content equivalent to 0.1 wt.% H_2O. This calculation is based upon a total (sum of three directions) integrated (area) absorbance of ~ 275 cm^{-1} of the O–H stretching band between 2750 and 3750 cm^{-1}, a sample thickness of ~ 0.02 cm, a density of 4.5 g/cm^3 and a molar absorption coefficient ε of ~ 80000 cm^{-2} per mol H_2O/L at an average wavenumber of ~ 3420 cm^{-1}.

X-ray crystallography

Single-crystal X-ray studies of a crystal from sample 2 were carried out with a Bruker APEX II diffractometer equipped with a CCD area detector using Mo$K\alpha$ (0.71073 Å) radiation, generator voltage and current of 50 kV and 30 mA, respectively, a crystal-to-detector distance of 50 mm and frame widths of 0.5° in ω and φ. Exposure time was 10 s for data collection. Data collection, refinement, and unit-cell parameters are given in Table 3. Atom coordinates, site occupancies, and equivalent isotropic displacement parameters are listed in Table 4 and anisotropic displacement parameters in Table 5 (not printed, freely available online, linked to this article on the GSW website of the journal, http://eurjmin.geoscienceworld.org/). Selected interatomic distances for perettiite-(Y) are reported in Table 6.

The perettiite-(Y) crystals show a tetragonal X-ray diffraction pattern (Fig. 5) but the structure could only be solved as a 50/50 pseudo-merohedral orthorhombic twin with the *a* and *c* axes having the same length. Structure solution (space group *Pmna* with $a = 12.8252(5)$, $b =$

Table 3. Parameters for X-ray data collection and crystal-structure refinement of perettiite-(Y).

Crystal data	
Unit-cell dimensions (Å)	$a = 12.8252(5)$ $b = 4.6187(2)$ $c = 12.8252(5)$
Volume ($Å^3$)	759.71(5)
Space group	*Pmna* (No. 53)
Z	2
Chemical formula	$(Y,Yb)_2(Mn,Ca)_4(Fe,Mg,Li)(Si_2B_8O_{24})$
Refined composition	$(Y_{0.82}Er_{0.18})_2(Mn_{0.83}Ca_{0.09}Y_{0.07})_4(Fe_{0.49}(Mg,Al)_{0.31}Li_{0.2})[Si_2B_{7.6}Be_{0.4}O_{24}]$
Intensity measurement	
Crystal shape	cube
Crystal size (mm)	0.2 × 0.2 × 0.2
Diffractometer	APEX II SMART
X-ray radiation	Mo$K\alpha$ $\lambda = 0.71073$ Å
X-ray power	50 kV, 30 mA
Monochromator	graphite
Temperature	293 K
Time per frame	10 s
Max. θ	36.3
Index ranges	$-21 \le h \le 21$ $-7 \le k \le 7$ $-21 \le l \le 19$
No. of measured reflections	31640
No. of unique reflections	1967
No. of observed reflections ($I > 2\sigma(I)$)	1814
Refinement of the structure	
No. of parameters used in refinement	108
R_{int}	0.0388
R_σ	0.0167
$R1$, $I > 2\sigma(I)$	0.0171
$R1$, all data	0.0210
w$R2$ (on F^2)	0.0445
GooF	1.072
$\Delta\rho_{min}$ (-e. $Å^{-3}$)	0.72 close to Si1
$\Delta\rho_{max}$ (e. $Å^{-3}$)	0.84 close to Y

Table 4. Atomic fractional coordinates, site occupancies, and isotropic equivalent displacement parameters (Å^2) for perettiite-(Y).

Site	Atom	Wyckoff positions	*x*	*y*	*z*	U_{eq}	Occupancy
Y	Y	4e	0.35558(2)	0	0.5	0.00521(5)	0.821(3)
Y	Er	4e	0.35558(2)	0	0.5	0.00521(5)	0.179(3)
Mn	Mn	8i	0.14192(2)	0.98143(5)	0.30187(3)	0.00966(9)	0.835(5)
Mn	Ca	8i	0.14192(2)	0.98143(5)	0.30187(3)	0.00966(9)	0.09
Mn	Y	8i	0.14192(2)	0.98143(5)	0.30187(3)	0.00966(9)	0.075(5)
Fe	Fe	2b	0	1	0.5	0.0078(2)	0.491(6)
Fe	Mg	2b	0	1	0.5	0.0078(4)	0.309(6)
Fe	Li	2b	0	1	0.5	0.0078(4)	0.2
Si1	Si	4h	0	0.52811(12)	0.14971(6)	0.00651(12)	1
B2	B	8i	0.28899(16)	0.4595(4)	0.34704(16)	0.0076(3)	1
B3	B	4f	0.1603(2)	0.5	0.5	0.0074(4)	1
B4	B	4h	0	0.4649(5)	0.6257(2)	0.0083(5)	0.8
B4	Be	4h	0	0.4649(5)	0.6257(2)	0.0083(5)	0.2
O1	O	4h	0	0.7740(4)	0.63492(14)	0.0104(3)	1
O2	O	8i	0.20560(11)	0.7644(2)	0.15130(10)	0.0080(2)	1
O3	O	4h	0.5	0.7727(4)	0.43761(14)	0.0095(3)	1
O4	O	8i	0.09281(9)	0.6758(2)	0.43019(10)	0.0106(2)	1
O5	O	4h	0	0.6838(3)	0.26614(14)	0.0098(3)	1
O6	O	8i	0.10245(10)	0.3198(3)	0.14049(10)	0.0093(2)	1
O7	O	8i	0.22729(10)	0.3152(2)	0.43376(10)	0.0093(2)	1
O8	O	4g	0.25	0.6726(3)	0.75	0.0115(3)	1

Table 6. Selected interatomic distances (Å) for perettiite-(Y).

Y coordination		Si1 coordination	
Y–O3 (2×)	2.2744(10)	Si1–O3	1.5907(19)
Y–O7 (2×)	2.3555(13)	Si1–O6(2×)	1.6328(13)
Y–O2 (2×)	2.3591(13)	Si1–O5	1.6573(19)
Y–O6 (2×)	2.3913(12)	Mean	1.628
Mean	2.345	B2 coordination	
Mn coordination		B2–O2	1.410(2)
Mn–O8	2.2175(11)	B2–O8	1.474(2)
Mn–O4	2.2577(13)	B2–O7	1.519(2)
Mn–O2	2.2781(14)	B2–O6	1.543(2)
Mn–O1	2.2904(11)	Mean	1.486
Mn–O2	2.3239(12)	B3 coordination	
Mn–O5	2.3265(10)	B3–O7(2×)	1.4791(19)
Mn–O6	2.6425(13)	B3–O4(2×)	1.4870(19)
Mn–O7	2.5369(13)	Mean	1.483
Mean	2.359	B4 coordination	
Fe coordination		B4–O1	1.432(3)
Fe–O1	2.0207(18)	B4–O4(2×)	1.534(2)
Fe–O1	2.0208(18)	B4–O5	1.548(3)
Fe–O4 (4×)	2.1119(12)	Mean	1.512
Mean	2.081		

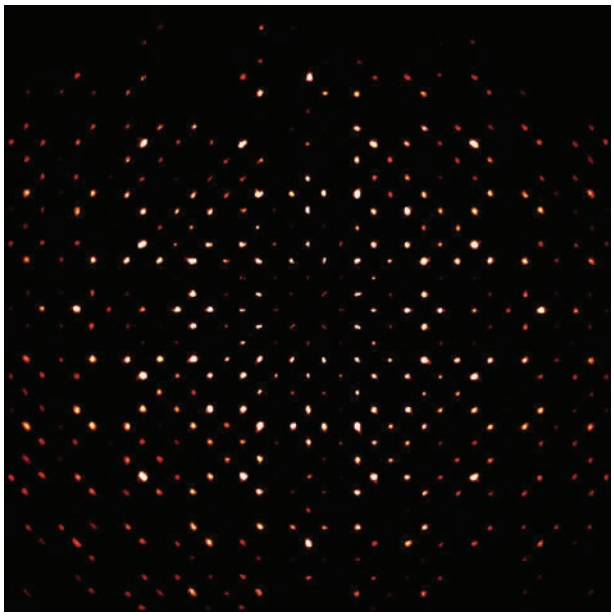

Fig. 5. Reconstruction of the *hk*0 reciprocal layer in tetragonal setting corresponding to *h*0*l* in space group *Pmna*. Note that there is no splitting of reflections indicating deviation from tetragonal symmetry, even at high θ values.

4.6187(2), $c = 12.8252(5)$ Å, $V = 759.71(5)$ Å^3, $Z = 2$) by direct methods and subsequent refinement with SHELXL (Sheldrick, 2008) converged at $R1 = 0.017$ with anisotropic displacement parameters for all sites. The occupancy of the Y site, showing the highest electron density in the structure, was refined with Y and Er scattering factors. The element Er represents the average atomic number of the lanthanoid distribution and Th + Zr content determined by LA-ICP-MS. The average analytically determined Ca content was fixed at the Mn site and Mn *versus* Y was refined to obtain full occupancy. Lithium from LA-ICP-MS results was assigned to the Fe site and held constant, allowing Mg to refine *versus* Fe to fill the octahedrally coordinated site. Due to similar X-ray scattering factors, Mg represents both Mg and minor Al. Test refinements with B4 fully occupied by B showed a significantly higher

Table 7. Calculated and measured PXRD data for perettiite-(Y).

h k l	$d_{calc.}$ (Å)	$I/I_{0\ calc.}$ (%)	Overlap	$d_{meas.}$ (Å)	$I/I_{0\ meas.}$ (%)
1 0 1	9.069	12.47		9.05	16.3
0 0 2	6.413	3.90		6.37	13.3
0 1 0	4.619	**40.92**		**4.63**	**51.7**
1 1 1	4.116	3.20			
3 0 1	4.056	**20.25**	x	**4.08**	**28.3**
1 0 3	4.056	**13.32**	x		
0 1 2	3.748	4.36			
2 1 0	3.748	6.41		**3.74**	**20.0**
2 1 1	3.597	2.36		3.61	11.7
2 1 2	3.236	4.52		3.24	15.0
4 0 0	3.206	6.29			
0 0 4	3.206	4.55			
1 1 3	3.047	**95.31**	x	**3.05**	**100.0**
3 1 1	3.047	**41.76**	x		
3 0 3	3.023	**37.48**	x		
2 0 4	2.868	2.85			
4 1 0	2.634	**65.23**	x	**2.64**	**66.7**
0 1 4	2.634	**49.96**	x		
3 1 3	2.529	**100.00**		**2.54**	**60.0**
4 1 2	2.436	3.81			
0 2 0	2.309	10.13		2.31	10.0
4 0 4	2.267	11.27		2.26	6.7
5 1 1	2.209	2.62		2.22	3.3
5 0 3	2.199	4.94			
2 2 1	2.142	5.42			
6 0 0	2.137	9.73	x	**2.12**	**23.3**
0 0 6	2.137	10.62	x		
2 1 5	2.117	18.95			
5 1 2	2.117	**20.71**			
4 1 4	2.035	9.34		2.02	10.0
1 2 3	2.007	7.76			
3 2 1	2.007	5.23			
6 1 0	1.940	12.46	x	1.93	8.3
0 1 6	1.940	12.56	x		
6 1 1	1.918	2.64			
4 2 0	1.874	16.71	x	**1.87**	**33.3**
0 2 4	1.874	13.16	x		
6 1 2	1.857	2.33			
4 1 5	1.838	2.12	x	**1.84**	**51.7**
3 2 3	1.835	**58.31**	x		
7 0 1	1.814	2.11			
1 0 7	1.814	11.57			
6 0 4	1.778	3.56			
4 0 6	1.778	6.00			
7 0 3	1.684	17.25	x	1.68	8.3
3 0 7	1.684	18.15	x		
6 1 4	1.660	8.79			
4 1 6	1.660	9.15			
4 2 4	1.618	12.44		1.62	6.7
8 0 0	1.603	8.17			
5 2 3	1.593	5.88			
3 1 7	1.582	**23.58**			
7 1 3	1.582	18.96			
0 2 6	1.569	12.65	x	**1.57**	**20.0**
6 2 0	1.569	10.71	x		
0 3 0	1.540	8.54		1.54	6.7
8 1 0	1.514	2.40			
6 0 6	1.511	6.42			
1 3 3	1.439	3.80	x	**1.44**	**25.0**
3 3 1	1.439	3.23	x		
1 2 7	1.426	3.66			
5 1 7	1.419	2.26			
6 2 4	1.409	2.37			
4 3 0	1.388	7.04	x	1.39	11.7
0 3 4	1.388	5.52	x		
3 3 3	1.372	10.04		1.37	13.3

U_{eq} value compared to the corresponding sites B2 and B3, suggesting that the assigned electron density was too high. In line with the slightly longer B4–O distances (Table 6) compared to B2–O and B3–O, Be determined by LA-ICP-MS was fixed at B4, which was then filled to full occupancy with B. The refined site occupancies from the crystal-structure determination yield the composition $(Y_{0.82}Er_{0.18})_2(Mn_{0.83}Ca_{0.09}Y_{0.07})_4(Fe_{0.49}(Mg,Al)_{0.31}Li_{0.2})[Si_2B_{7.6}Be_{0.4}O_{24}]$.

X-ray powder diffraction data are listed in Table 7. A Gandolfi-like measured pattern was produced by a total of six 300 s φ scans of 300° at θ values of −27.44, 0.35, and 28.14° with $\chi = 90°$ and corresponding ones with $\chi = 0°$ (camera distance = 66.2 mm). Data collection and reduction was done with CrysAlisPro, Agilent Technologies, version 1.171.37 using a SuperNova (Mo) X-ray Source. Intensities were estimated from maximum peak heights. The calculated pattern produced from coordinates and occupancies of the structure refinement for Debye-Scherrer geometry and Cu*K*α X-radiation was generated using the program LAZYPULVERIX (Yvon *et al*., 1977). The eleven strongest lines are shown in bold in Table 7.

Discussion

Crystal structure

The crystal shows a tetragonal diffraction pattern (Fig. 5) but optical inspection indicated 90° rotational twinning around the short 4.6 Å axis, supporting orthorhombic symmetry with $a = c = 12.8252(5)$ Å. This case can be classified as metric merohedry according to Nespolo & Ferraris (2000). Other examples of this kind are reported, *e.g*. for the structures of semenovite-(Ce), bismutite, beyerite and kettnerite (Mazzi *et al*., 1979; Grice *et al*., 1999; Grice, 2002).

The excellent structure refinement ($R1 = 0.017$) identifies for perettiite-(Y) tetrahedral sheets parallel to (010) with 4-, 5- and 8-membered rings (Fig. 6) of simplified $Si_2B_8O_{24}$ composition, sandwiching three interlayer sites. Two of those are 8-coordinated and one represents a regular octahedron. One eight-coordinated site is occupied by Y^{3+} and lanthanoids (Fig. 6). Light REE are depleted compared to the heavy ones according to the REE plot reported in Fig. 7. A marked negative Eu anomaly is evident. The chondrite normalizing factors were taken from McDonough & Sun (1995). An additional eight-coordinated site is dominated by Mn^{2+} with additional Ca^{2+} and Y^{3+}. Considering atomic distances (Table 6), the two eight-coordinated sites have the same size allowing, in principle, mixed occupancies between $(Y, Ln)^{3+}$ and $(Mn, Ca)^{2+}$ cations. Nevertheless, the $(Y, Ln)^{3+}$ site is strongly favored by trivalent cations on the basis of bond-valence calculations (Brown & Altermatt, 1985) listed in Table S2 (supplementary material). The O3 site (Fig. 6) has one bond to Si^{4+} and two bonds to $(Y, Ln)^{3+}$ leading to a bond valence sum (bvs) of ∼ 2, which prohibits any

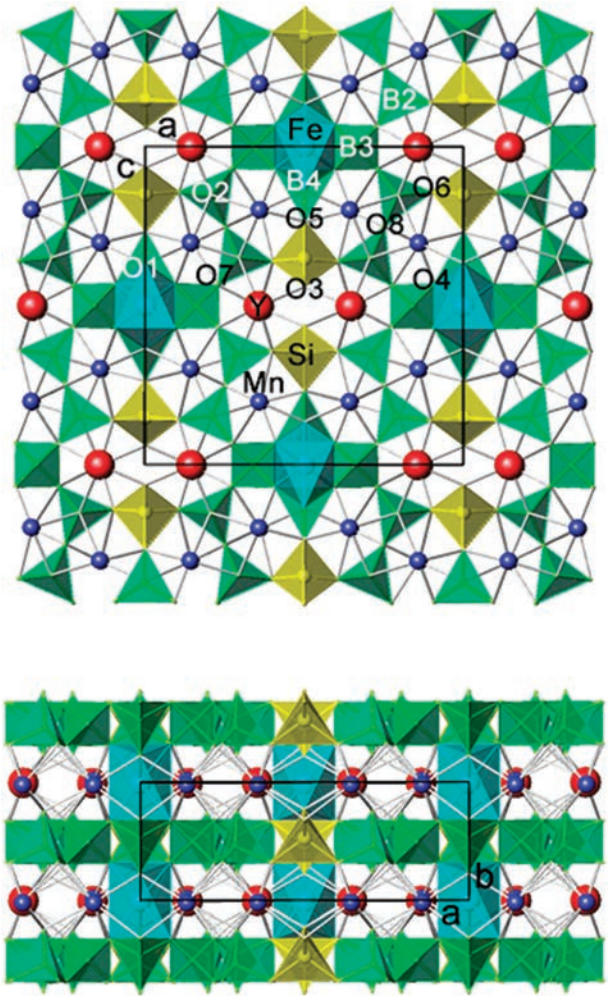

Fig. 6. The tetrahedral sheet in perettiite-(Y) (SiO_4 tetrahedra yellow, BO_4 tetrahedra green). The interlayer octahedron (Fe, Mg, Li) between the 4-membered rings of BO_4 tetrahedra is shown in light blue. The Mn^{2+}-rich interlayer sites are shown in blue, Y and lanthanoids interlayer sites in red. Oxygen and boron sites are labeled. Unit-cell outlines are shown.

substitution by divalent cations to avoid underbonding. On the other hand, the oxygen at O5 (Fig. 6) is shared with Si^{4+} at Si1 and B^{3+} at B4. The latter is partially substituted by Be^{2+} as confirmed by atomic distances and reasonable anisotropic displacement parameters if Be^{2+} is introduced as an additional tetrahedral occupant to the refinement model. This charge deficiency has to be balanced by a bond to a trivalent cation in the interlayer leading to the heterovalent substitution: $Mn^{2+} + B^{3+} \rightarrow Y^{3+} + Be^{2+}$. This explains the partial substitution of Y^{3+} at the Mn site. An octahedral site in the interlayer, bonded to the 4-membered rings of BO_4 tetrahedra (B2, B3), is occupied by Fe^{2+} and Mg^{2+} with additional Li^{+}. The bond valence calculations confirm the presence of divalent Fe, in agreement with the Fe^{2+}–O atomic distances in a corresponding topological environment described for the beryllosilicate homilite (Miyawaki *et al*., 1984). The Fe^{2+} ion is partially substituted by Mg^{2+} as shown (Fig. 8) by the inverse correlation between Fe^{2+} and Mg^{2+}. Electron-microprobe analyses indicated crystal zoning with Mg increasing from core to rim.

The role of minor Al (*ca*. 0.1 Al *pfu*) is not clear, but stoichiometry arguments based on the chemical composition suggest tetrahedral Al (replacing B and Si). However, site occupancy refinements (crystal structure) exclude Al replacing B. Due to similar X-ray scattering factors for Si and Al, Al for Si replacement cannot be rejected. If all Al is assigned to the SiO_4 tetrahedron, this would only amount to 5 %, leading to an insignificant increase of the average Si–O bond length. Alternatively, Al occupies the octahedral interlayer site together with Fe, Li and Mg.

Relationship to other species

The mineral and its crystal structure are unique (Fig. 6). However, there are several minerals with a similar short axis (*ca.* 4.7 Å or multiple values) perpendicular to tetrahedral sheets (Miyawaki & Nakai, 1996). A good

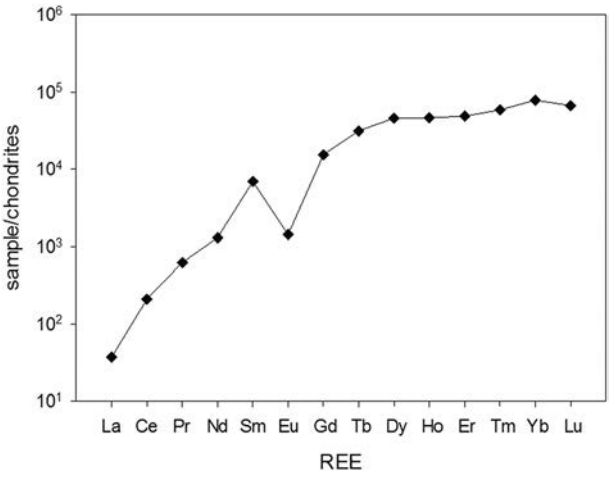

Fig. 7. Chondrite-normalized REE pattern for perettiite-(Y). The chondrite normalizing factors are taken from McDonough & Sun (1995).

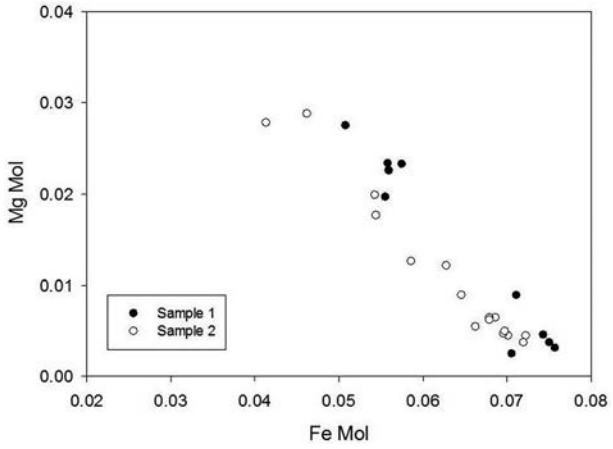

Fig. 8. Fe *vs*. Mg plot from EMPA showing homovalent substitution $Fe^{2+} \rightarrow Mg^{2+}$ as indication of crystal zoning within perettiite-(Y). Mol corresponds to wt.% oxide/molecular weight; to obtain pfu (normalized to 2 Si apfu) values have to be multiplied by 10.3.

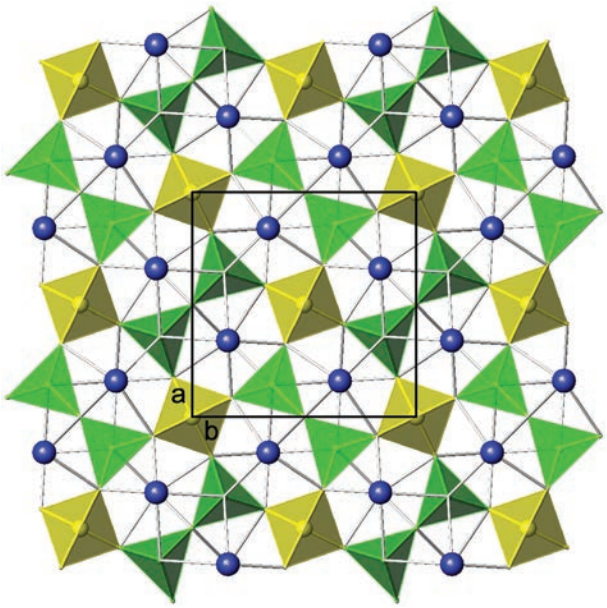

Fig. 9. The okayamalite (melilite group) tetrahedral sheet (Giuli *et al*., 2000). Tetrahedral SiO_4 and BO_4 units are indicated in yellow and green, respectively. Ca interlayer sites are in blue. Unit-cell outlines are shown.

example is the melilite group as exemplified by okayamalite $Ca_2[SiB_2O_7]$, tetragonal, space group $P\bar{4}2_1m$, a = 7.12, c = 4.81 Å (Giuli *et al*., 2000). The interlayer is mainly occupied by Ca (Fig. 9). The structure of melilite-type compounds is characterized by an arrangement of corner-sharing tetrahedra forming 5-membered rings parallel to (001).

Monoclinic minerals of the datolite and gadolinite series, space group $P2_1/c$ (a = 4.7, b = 7.6, c = 9.8 Å, β = 90.5°) have tetrahedral sheets built by BO_4, BeO_4, and SiO_4 tetrahedra with interlayer Ca, Y, and lanthanoids polyhedra. Gadolinite (Fig. 10), $REE^{3+}{}_2Fe^{2+}[Be_2Si_2O_{10}]$, has a beryllosilicate sheet (Miyawaki *et al*., 1984) and homilite, $Ca_{2.00}(Fe_{0.90}Mn_{0.03})[B_{2.00}Si_{2.00}O_{9.86}(OH)_{0.14}]$, a borosilicate sheet (Miyawaki *et al*., 1985) characterized by 4- and 8-membered rings.

Tetrahedral sheets with 4-, 5- and 8-membered rings as in perettiite-(Y) can be found in hellandite, semenovite-(Ce), harstigite and nordite-(La) (Bakakin *et al*., 1970; Mazzi *et al*., 1979; Hesse & Stümpel, 1986; Oberti *et al*., 1999). The hellandite minerals are monoclinic, space group $P2/a$, a = 19, b = 4.7, c = 10.3 Å, β = 111.4° (Oberti *et al*., 1999). The group comprises hellandite (Fig. 10), $(Ca,Y)_6(Al,Fe)[(OH)_2|Si_4B_4O_{20}(OH)_2]$, and tadzhikite-(Y), $Ca_2(Ca,Y)_2(REE^{3+},\square)_2(Ti,Fe^{3+})[(OH)_2|Si_4B_4O_{20}(OH)_2]$. In particular, tadzhikite-(Y) has $Si_4B_4O_{16}(O,OH)_6$ sheets with interlayer Ca, Y, and Fe^{3+}, Ti ions.

The structure of semenovite-(Ce) (Mazzi *et al*., 1979), $(Fe^{2+},Mn,Zn,Ti)REE_2Na_{0-2}(Ca,Na)_8(Si,Be)_{20}(O,OH,F)_{48}$, Z = 2, orthorhombic, a = 13.879(5), b = 13.835(5) c = 9.942(6)Å, space group *Pmnn*, is topologically similar to perettiite-(Y). In semenovite, the interlayer octahedron (Fe, Mn) between the 4-membered rings of SiO_4 tetrahedra and also the eight-coordinated interlayer (Ca, Na) and (Ce,

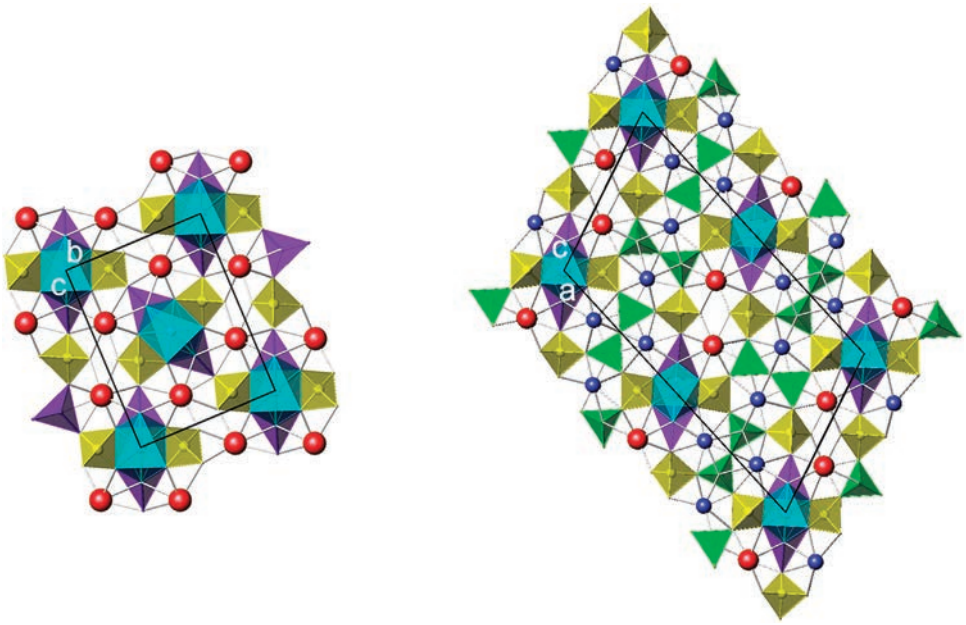

Fig. 10. **Left (a)**: The tetrahedral sheet in gadolinite-(Y) (SiO_4 tetrahedra yellow, BeO_4 tetrahedra violet; Miyawaki *et al*., 1984). The interlayer octahedron (Fe) between the 4-membered rings of BeO_4 and SiO_4 tetrahedra is shown in light blue, Y and lanthanoids interlayer sites in red. Unit-cell outlines are shown. **Right (b)**: The tetrahedral sheet in hellandite-(Y) (SiO_4 tetrahedra yellow, BO_4 tetrahedra green, BeO_4 tetrahedra violet; Oberti *et al*., 1999). The interlayer octahedron (Al, Fe) between the 4-membered rings of BeO_4 and SiO_4 tetrahedra is shown in light blue. Interlayer Ca (blue) and Y (red) are indicated by spheres.

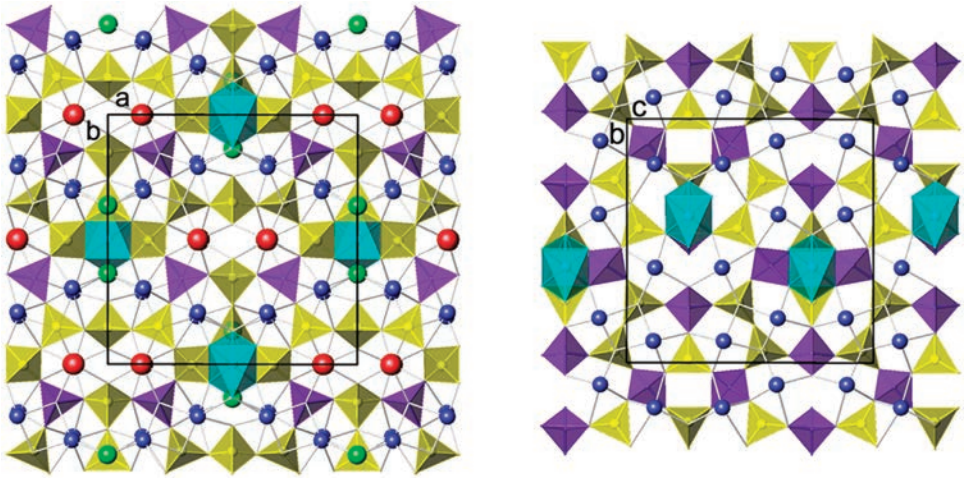

Fig. 11. **Left (a)**: The tetrahedral sheet in semenovite-(Ce) (SiO_4 tetrahedra yellow, BeO_4 tetrahedra violet; Mazzi *et al*., 1979). The interlayer octahedron (Fe, Mn) between the 4-membered rings of SiO_4 tetrahedra is shown in light blue. Interlayer (Ca, Na) and (Ce, Na) are indicated by blue and red spheres, respectively. Tetrahedral corners emphasized by green spheres represent F. **Right (b)**: The tetrahedral sheet in harstigite (Si tetrahedra yellow, BeO_4 tetrahedra violet; Hesse & Stümpel, 1986). Only half the unit-cell along [100] is shown. The adjacent sheet of tetrahedra (not shown) is shifted relative to the displayed reference sheet. The interlayer octahedron (Mn) between the 4-membered rings of BeO_4 and SiO_4 tetrahedra is shown in light blue. Interlayer Ca sites are blue. Unit-cell outlines are shown.

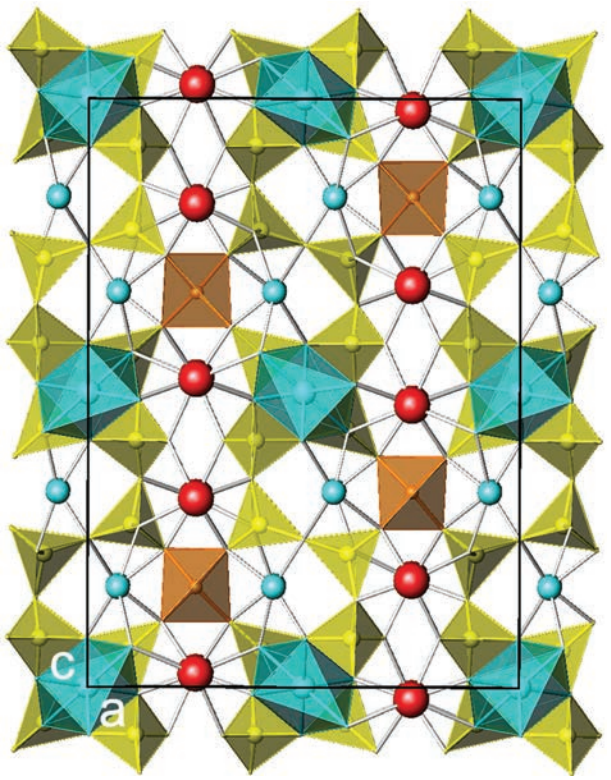

Fig. 12. The tetrahedral sheet in nordite-(La) (Si tetrahedra yellow, (Zn, Mg, Fe)O_4 tetrahedra orange; Bakakin *et al*., 1970). The interlayer octahedron (Na,Mn)O_6 between the 4-membered ring of SiO_4 tetrahedra is shown in light blue. Interlayer Na is indicated by blue spheres while interlayer (La,Ce) and (Sr,Ca) sites are colored red.

Na) cation sites correspond to those in perettiite-(Y) (Fig. 11). In contrast to perettiite-(Y), semenovite-(Ce) exhibits twice the translation ($c = 9.942(6)$ Å) perpendicular to the sheets, which is explained by different vacancy distributions in the two interlayer units. The origin of the sector twinning responsible for the tetragonal pseudosymmetry in semenovite-(Ce) is explained by Mazzi *et al*. (1979) on a structural basis. This explanation may also be extended to perettiite-(Y).

The beryllosilicate sheets of harstigite (Hesse & Stümpel, 1986), $MnCa_6Be_4[SiO_4]_2[Si_2O_7]_2(OH)_2$ (orthorhombic with space group *Pnam*, $a = 9.793(2)$, $b = 13.636(3)$, $c = 13.830(3)$ Å, $Z = 4$) are topologically similar to semenovite-(Ce) and perettiite-(Y) with the difference that they are not superimposed in an identical fashion along *a* (Fig. 11), but displaced relatively to each other.

The tetrahedral sheet of nordite (Bakakin *et al*., 1970), $Na_{2.8}Mn^{2+}_{0.2}Sr_{0.5}Ca_{0.5}La_{0.5}Ce_{0.4}Zn_{0.4}Mg_{0.3}Mn^{2+}_{0.2}Fe^{2+}_{0.1}Si_{5.9}Fe^{3+}_{0.2}O_{17}$ (space group *Pcca*, $a = 14.27(3)$ $b = 5.16(1)$ $c = 19.45(15)$ Å, $Z = 4$), is composed of strongly undulating silicate chains parallel to [001] connected along [100] by large (Zn, Mg, Fe)O_4 tetrahedra leading to the same kind of 4-, 5- and 8-membered rings as in the above structures but with a different frequency in the unit-cell (Fig. 12).

Acknowledgments: We thank R. Widmer for performing the microindentation test, A. Dielforder for preliminary EDX analysis, J. Hauser and P. Macchi for the Gandolfi-like measured powder pattern, A. Lanza and G. Cametti for fruitful discussions.

References

Bakakin, V.V., Belov, N.V., Borisov, S.V., Solovyeva [Solov'eva], L.P. (1970): The crystal structure of nordite and its relationship to melilite and datolite-gadolinite. *Am. Mineral.*, **55**, 1167–1181.

Brown, I.D. & Altermatt, D. (1985): Bond-valence parameters obtained from a systematic analysis of the Inorganic Crystal Structure Database. *Acta Cryst.*, **B41**, 244–247.

Falster, A.U., Peretti, A., Simmons, W.B. (2008): Mushroom tourma and associated minerals from pegmatites near Momeik, Mogok stone tract, Myanmar (Burma). The 24th technical session of the Rochester Mineralogical Symposium (RMS). *Rocks and Minerals*, **83**, 342.

Farmer, V.C. (ed) (1974): The Infrared Spectra of Minerals. Miner. Soc., London, 539 p.

Giuli, G., Bindi, L., Bonazzi, P. (2000): Rietveld refinement of okayamalite, $Ca_2SiB_2O_7$: structural evidence for the B/Si ordered distribution. *Am. Mineral.*, **85**, 1512–1515.

Grice, J.D. (2002): A solution to the crystal structures of bismutite and beyerite. *Can. Mineral.*, **40**, 693–698.

Grice, J.D., Cooper, M.A., Hawthorne, F.C. (1999): Crystal-structure determination of twinned kettnerite. *Can. Mineral*, **37**, 923–927.

Guillong, M., Hametner, K., Reusser, E., Wilson, S.A., Günther, D. (2005): Preliminary characterisation of new glass reference materials (GSA-1G, GSC-1G, GSD-1G and GSE-1G) by Laser Ablation-Inductively Coupled Plasma-Mass Spectrometry using 193 nm, 213 nm and 266 nm wavelengths. *Geostand. Geoanal. Res.*, **29**, 315–331.

Hesse, K.F. & Stümpel, G. (1986): Crystal structure of harstigite, $MnCa_6Be_4[SiO_4]_2[Si_2O_7]_2(OH)_2$. *Z. Kristallogr.*, **177**, 143–148.

Keller, P.C. (1983): The rubies of Burma: A review of the Mogok stone tract. *Gems & Gemol.*, **19**, 209–219.

Kroslakova, I. & Günther, D. (2007): Elemental fractionation in laser ablation-inductively coupled plasma-mass spectrometry: evidence for mass load induced matrix effects in the ICP during ablation of a silicate glass. *J. Anal. at. Spectrom.*, **22**, 51–62.

Libowitzky, E. & Rossman, G.R. (1997): An IR absorption calibration for water in minerals. *Am. Mineral.*, **82**, 1111–1115.

Longerich, H.P., Jackson, S.E., Günther, D. (1996): Laser ablation inductively coupled plasma mass spectrometric transient signal data acquisition and analyte concentration calculation. *J. Anal. at. Spectrom.*, **11**, 899–904.

Lussier, A.J., Aguiar, P.M., Michaelis, V.K., Kroeker, S., Herwig, S., Abdu, Y., Hawthorne, F.C. (2008): Mushroom elbaite from the Kat Chay mine, Momeik, near Mogok, Myanmar: I. Crystal chemistry by SREF, EMPA, MAS NMR and Mössbauer spectroscopy. *Mineral. Mag.*, **72**, 747–761.

Mazzi, F., Ungaretti, L., Dal Negro, A., Peterson, O.V., Rønsbo, J.G. (1979): The crystal structure of semenovite. *Am. Mineral.*, **64**, 202–210.

McDonough, W.F. & Sun, S.S. (1995): The composition of the earth. *Chem. Geol.*, **120**, 223–253.

Miyawaki, R. & Nakai, I. (1996): Crystal chemical aspects of rare earth minerals. *in* ''Rare Earth Minerals'', A.P. Jones, F. Wall, C.T. Williams, ed. Mineralogical Society Series No. 7, Chapman & Hall Publishing, London 21–40.

Miyawaki, R., Nakai, I., Nagashima, K. (1984): A refinement of the crystal structure of gadolinite. *Am. Mineral.*, **69**, 948–953.

—, —, — (1985): Structure of homilite, $Ca_{2.00}(Fe_{0.90}Mn_{0.03})B_{2.00}Si_{2.00}O_{9.86}(OH)_{0.14}$. *Acta Cryst.*, **C41**, 13–15.

Nespolo, M. & Ferraris, G. (2000): Twinning by syngonic and metric merohedry. Analysis, classification and effects on the diffraction pattern. *Z. Kristallogr.*, **215**, 77–81.

Novák, M., Sejkora, J., Škoda, R., Budina, V. (2008): Bismutotantalite-stibiotantalite-stibiocolumbite assemblage from elbaite pegmatites at Molo near Momeik, northern Shan State, Myanmar. *N. Jb. Miner. Abh.*, **185**, 17–26.

Oberti, R., Ottolini, L., Camara, F., Della Ventura, G. (1999): Crystal structure of nonmetamict Th-rich hellandite-(Ce) from Latium (Italy) and crystal chemistry of the hellandite-group minerals. *Am. Mineral.*, **84**, 913–921.

Peretti, A. (2013): GRS expeditions to the Mogok ruby, sapphire and spinel mines. *Jewellery News Asia*, October, 54–58.

Peretti, A., Danisi, R.M., Armbruster, T., Guenther, D., Wang, H., Bieri, W., Mullis, S., Ngwe Lin, Tun, Myo Myint, Oo. (2015): Geology and mineralogy of pegmatites from Khetchel (Burma, Myanmar) containing Perettiite-(Y). *Contrib. Gemol.*, **13**, 1–20.

Pouchou, J.L., Pichoir, F. (1984): A new model for quatitative X-ray microanalysis, Part II: Application to in-depth analysis of heterogeneous samples. *Rech. Aerospatiale*, **1984–5**, 47–65.

Rossman, G.R. (1988): Vibrational spectroscopy of hydrous components. *Rev. Mineral.*, **18**, 193–206.

Searle, M.P., Noble, S.R., Cottle, J.M., Waters, D.J., Mitchell, A.H.G., Hlaing, T., Horstwood, M.S.A. (2007): Tectonic evolution of the Mogok metamorphic belt, Burma (Myanmar) constrained by U-Th-Pb dating of metamorphic and magmatic rocks. *Tectonics*, **26**, 1–24.

Sheldrick, G.M. (2008): A short history of SHELX. *Acta Cryst.*, **A64**, 112–122.

Yvon, K., Jeitschko, W., Parthé, E. (1977): LAZY PULVERIX, a computer program, for calculating X-ray and neutron diffraction powder patterns. *J. Appl. Cryst*, **10**, 73–74.

Zaw, K. (1998): Geological evolution of selected granitic pegmatites in Myanmar (Burma): Constraints from regional setting, lithology, and fluid-inclusion studies. *Intern. Geol. Rev.*, **40**, 647–662.

Received 23 June 2015
Modified version received 8 July 2015
Accepted 9 July 2015